European Journal of Chemistry

Check for updates

View Journal Online
View Article Online

Effective removal of arsenic (V) from aqueous solutions using efficient CuO/TiO_2 nanocomposite adsorbent

Saima Farooq [1], Asima Siddiqa [2,*], Sobia Ashraf [3], Sabtain Haider [4], Saiqa Imran [5], Shabnam Shahida [3] and Sara Qaisar [2]

[1] *Department of Biological Sciences and Chemistry, College of Arts and Sciences, University of Nizwa, Nizwa 616, Oman*
[2] *Nanosciences and Technology Department, National Centre for Physics, Islamabad, 44000, Pakistan*
[3] *Department of Chemistry, The University of Poonch Rawalakot, Azad Kashmir, Pakistan*
[4] *Department of Chemistry, Quaid-i-Azam University, Islamabad, 45320, Pakistan*
[5] *Pakistan Council of Research in Water Resources, Ministry of Science and Technology, Islamabad, Pakistan*

* *Corresponding author at: Nanosciences and Technology Department, National Centre for Physics, Islamabad, 44000, Pakistan.*
e-mail: asima.siddiqa@ncp.edu.pk (A. Siddiqa).

RESEARCH ARTICLE

10.5155/eurjchem.13.3.284-292.2283

Received: 05 May 2022
Received in revised form: 07 June 2022
Accepted: 11 June 2022
Published online: 30 September 2022
Printed: 30 September 2022

KEYWORDS

TiO_2
CuO/TiO_2
Adsorption
Arsenate ion removal
Hybrid nanocomposite
Water purification system

ABSTRACT

The groundwater is one of the biggest natural resources for providing drinking water to millions of people all around the globe. However, the presence of large amount of arsenic(V) in water causes serious health hazards to the consumers which necessitates the development of cost-effective remediation. The CuO/TiO_2 nanocomposites were prepared by the precipitation-deposition method for the removal of the arsenate ion (AsO_4^{3-}) from water. The prepared samples were characterized by powder X-ray diffraction, Fourier transform infrared, and scanning electron microscopy to examine crystallite size and structure, material purity, textural features, morphology, and surface area. The effect of different operating parameters such as pH, contact time, initial concentration of arsenic(V) and nanocomposite dose on the removal rate of arsenic(V) was examined to optimize the adsorption performance of the CuO/TiO_2 nanocomposite. In addition, the adsorption mechanism was studied by employing Langmuir and Freundlich adsorption isotherms to gain better understanding of the adsorption mechanism. The Freundlich adsorption isotherm fits well with the experimental data and the maximum adsorption capacity of the Langmuir model was found to be 90 mg/g for arsenic(V). The CuO/TiO_2 nanocomposite shows remarkable adsorption performance for the treatment of arsenic(V) contaminated water samples. This study provides a cost-effective solution for the safe use of groundwater contaminated with arsenic.

Cite this: *Eur. J. Chem.* **2022**, *13(3)*, 284-292 **Journal website**: www.eurjchem.com

1. Introduction

Arsenic (As) is the third most toxic element that comprises approximately 1.8 ppm of the Earth's crust [1]. It is the major constituent of 200 mineral species having formula MAsS and MAs_2 (where M = Fe, Co, Ni) such as arsenopyrite (FeAsS), orpiment (As_2S_3), and realgar (AsS) [2]. The natural activities (such as weathering of rocks, forest fires and volcanic events) and anthropogenic sources (like pesticides, herbicides, mining, copper smelting, chemical warfare agents and fossil fuel burning) are held responsible for the release of arsenic in the air, water and soil [2-4]. In the environment, arsenic exposure to human system may occur through inhalation in the air, absorption through the skin, or ingestion of contaminated food and water. However, contaminated water is the most lethal route. In 2012, almost 200 million people throughout the world were exposed to drinking water having As concentration above 50 ppb [5]. This situation is even worser in Asian countries specifically in Bangladesh, China, India, and Pakistan. Human exposure to arsenic in these countries is constantly increasing, due to the excessive release of As-rich untreated industrial effluent, inadequate wastewater treatment processes, poor health facilities, lack of water quality surveillance, and public ignorance [6,7]. Arsenic causes skin lesions, respiratory diseases, mutagenic changes, and tumours depending on the proportion and duration of exposure [8,9]. As a result, the International Agency for Research on Cancer (IARC) has classified it as a class 1 human carcinogen substance. In 1993, the United States Environmental Protection Agency (US-EPA) and World Health Organization (WHO) reduced the permissible arsenic level in drinking water from 50 to 10 ppb [3]. This drastic decrease sets an alarming condition for the regulatory authorities in every corner of the world.

In our environment, arsenic exists in either organic or inorganic form. In groundwater, arsenic occurs mainly in inorganic form (as oxyanions) such as arsenite As(III) and arsenate As(V) which are much more noxious than organic form [10]. However, As(V) is less poisonous in comparison to As(III) but it is thermodynamically more stable due to its preponderate as a major arsenic constituent of groundwater. Therefore, it is

https://dx.doi.org/10.5155/eurjchem.13.3.284-292.2283

the need to develop an economical and effective method for arsenate removal [11]. Researchers have employed conventional methods for the treatment of As(V) present in water like advanced oxidation process, bioremediation, adsorption, membrane filtration technologies, electrochemical methods and ion-exchange process [3,4,6,12-14]. Among those, adsorption has been considered as an efficient method owing to its prominent features i.e., high efficiency, availability, profitability, cost-effectiveness, regeneration of adsorbent and ease in operation. The process simply involves the segregation of toxins from water and accretion of them on the adsorbent surface by physical or chemical interaction. This technique is easy to operate and equally effective in the removal of toxic pollutants even at low concentrations [15]. Several adsorbents such as dry plants, red mud, zeolites, hydrotalcite, rice husk and natural clays have been employed for the removal of arsenic [16,17]. However, most of these adsorbents have shown poor adsorption capacity for As(V) and also face difficulty in regeneration.

The adsorption capacity is highly dependent on the nature, texture, size, and shape of the adsorbent. Therefore, researchers have turned their attention toward the development of hybrid nanomaterial composites for environmental remediation owing to their enhanced surface area, more active sites, higher selectivity, and ease in regeneration [18]. In recent years, TiO_2 has been extensively investigated for the removal of As due to its low toxicity, higher chemical and thermal stability, low generation cost and high selectivity for As. However, low surface area and higher agglomeration have limited TiO_2 performance [19]. Recently, researchers have found that TiO_2 based nanocomposites come with a large surface area and a higher adsorption rate. Feng et al. [20] reported an improved removal efficiency of As(III) and As(V) over Fe_3O_4@SiO_2@TiO_2 from wastewater released during the gold cyanide process. Sagharloo *et al.* [21] studied the removal of arsenic from contaminated water using immobilized ZnO/TiO_2 AC. Along with TiO_2, CuO nanoparticles have gained much attention for improving the adsorption efficiency of different nanosorbents for arsenic removal by making hybrid composites. Malwal *et al.* [22] reported the increased removal efficiency of As(III) over the CuO/ZnO nanocomposite. Sharma *et al.* [23] prepared a CuO/ZnO nanocomposite with an enhanced adsorption rate for Cr(VI) and Pb(II) along with improved photocatalytic degradation of basic violet and reactive yellow. Bhattacharya *et al.* [24] reported the removal of ciprofloxacin over CuO/TiO_2 nanocomposite. Furthermore, to our knowledge, the CuO/TiO_2 nanocomposite has not yet been used to remove As(V) from aqueous media.

In the present work, CuO/TiO_2 nanocomposites were prepared by the precipitation-deposition method. The characterization of prepared samples was done by employing X-ray powder diffraction (XRD), Fourier transform infrared (FT-IR), and Scanning electron microscopy (SEM). The adsorption potential of the CuO/TiO_2 nanocomposite toward As(V) under different parameters such as pH, contact time, arsenic ion concentration, and the adsorbent dose was investigated. The isothermal studies and regeneration capacity of nanocomposite were also studied. The result of this work helps develop a cost-effective solution for the removal of arsenic from groundwater.

2. Experimental

2.1. Reagents

All chemicals were analytical grade and were used without further purification. Commercial titania powder (anatase TiO_2, 99.7%), copper nitrate trihydrate ($Cu(NO_3)_2{\cdot}3H_2O$, 99%), hydrochloric acid (HCl, 37%), ethanol (C_2H_5OH, 99.8%), sodium hydroxide (NaOH, 98%), and sodium arsenate dibasic hepta hydrate ($Na_2HAsO_4{\cdot}7H_2O$, 98%) were purchased from Sigma-Aldrich, USA. Distilled water was used throughout the study.

2.2. Synthesis of CuO/TiO_2 nanocomposites

CuO/TiO_2 nanocomposites were synthesized by the previously reported precipitation-deposition method [25]. First, the required amount (0.3, 0.5 and 0.9 g) of titania was dissolved separately in 20 mL of ethanol and stirred in each suspension for 24 hours to completely disperse the TiO_2 in the solvent. Second, 20 mL of different molar solutions (i.e., 0.02, 0.04 and 0.06 M) of copper nitrate were prepared in distilled water. Then, add 20 mL of 0.02 M copper nitrate solution in 0.3 g/20 mL ethanol TiO_2 suspension and left on stirring for an hour to obtain a homogenous mixture. Subsequently, the pH of the mixture was adjusted to 10 by adding 1 M sodium hydroxide solution dropwise and stirring until black precipitates formed. The precipitates were extracted by centrifugation and rinsed several times with distilled water to neutralize the pH. Finally, the precipitates obtained were dried in an oven at 90 °C for 8 hours and then calcined for 3 hours at 400 °C. In this way, the nanocomposite of CuO/TiO_2 was obtained. A series of nanocomposites (1, 3 and 5 wt % CuO/TiO_2) were synthesized by the same procedure by simply varying concentrations of $Cu(NO_3)_2{\cdot}3H_2O$ solution and TiO_2 suspension.

2.3. Characterization

The crystal structure, phase, and size of the prepared nanocomposite materials were analysed using a powder X-ray diffractometer (Bruker D_8 Advance X-ray diffractometer) employing CuKα radiation in the 2θ range of 20-80° at a scan rate of 0.02°/sec. The functional group and phase purity of all samples were analysed using Fourier transform infrared spectra recorded on a Jasco 1106 spectrophotometer in the range of 500-4000 cm^{-1} using a KBr disk. The microstructure and morphology were studied by scanning electron microscopy (SEM LEO 1430 VP, Germany) on gold-coated surfaces.

2.4. Batch adsorption experiments

The stock solution (1000 ppb) of As(V) was prepared by dissolving the stoichiometric amount of sodium arsenate dibasic heptahydrate in distilled water and the required dilution was made in the same solvent. A series of batch experiments were performed to study the effect of pH of solution, contact time, arsenic ion concentration and adsorbent dose on the removal of As(V) from aqueous solution using the prepared CuO/TiO_2 nanocomposite. These experiments were carried out in 250 mL glass beaker containing 100 mL of varying initial concentration (100-1000 ppb) of aqueous As(V) solution at different pH (1-9) and nanocomposite dosages (0.05 to 0.30 g). All these experiments were carried out at room temperature and solutions were stirred for different time intervals (1-6 h) in dark. After adsorption, collected samples were centrifuged and filtered to separate nanocomposite. Finally, the filtrate was analysed by using hydride generated atomic absorption spectrophotometer (Vario 06, Germany) to obtain optimized nanocomposite dosage and As(V) concentration. This instrument can measure arsenic even at a very low concentration as it employed sodium borohydride (as a reducing agent) which converts arsenic into an arsine gas. The concentration of arsenic is detected as a function of amount of arsine gas produced [26]. The adsorption capacity of nanocomposite (Q_e) and percentage removal efficiency (%R) was calculated by employing Equations (1 and 2) given below [27]:

$$Q_e = \frac{(C_0 - C_e)}{M} \times V \quad (1)$$

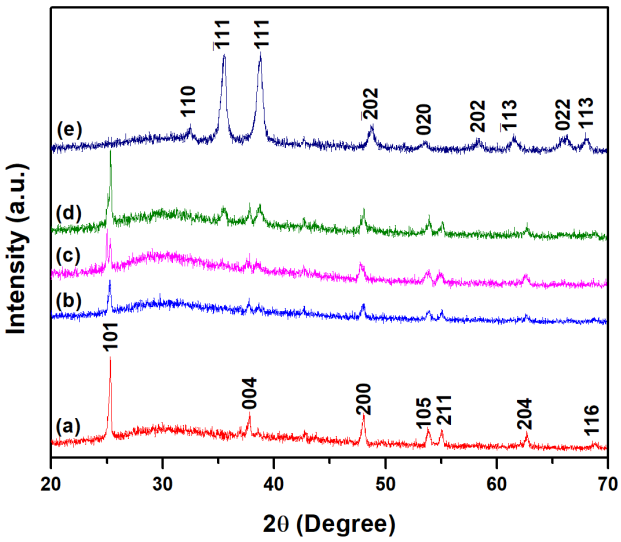

Figure 1. XRD spectra of (a) TiO_2, (b) 1wt. % CuO/TiO_2, (c) 3wt. % CuO/TiO_2, (d) 5wt. % CuO/TiO_2 and (e) CuO.

$$\%R = \frac{(C_0 - C_e)}{C_0} \times 100 \quad (2)$$

where Q_e is the adsorbate amount adsorbed per gram of adsorbent at equilibrium (mg/g), C_0 and C_e are the initial and equilibrium concentration of adsorbate (mg/L), V is the volume of solution (L), M is the mass of adsorbent (g) and %R represents the overall removal of adsorbate based on the ratio of adsorbent dosage to adsorbate volume at a particular adsorbate concentration.

2.5. Isothermal analysis

The adsorption and desorption isotherms were also investigated by using the well-known Langmuir and Freundlich isotherm model. The Langmuir isotherm is described by using the Equation (3) as follows;

$$\frac{1}{Q_e} = \frac{1}{Q_{max}} + \frac{1}{KC_eQ_{max}} \quad (3)$$

where Q_e is the adsorption capacity of the adsorbent (mg/g), and C_e is the equilibrium concentration of adsorbate (mg/L). K is the Langmuir constant (L/mg) which is related to adsorption energy and Q_{max} is the optimum adsorption capacity of adsorbent (mg/g) was calculated from the slope (1/K) and intercept values ($1/Q_{max}$) of Langmuir plot [28].

The important characteristics of the Langmuir isotherm are expressed in terms of the dimensionless equilibrium parameter (R_L).

$$R_L = \frac{1}{1 + KQ_{max}} \quad (4)$$

The R_L value defines adsorption as irreversible ($R_L = 0$), favourable ($1 > R_L > 0$), linear ($R_L = 1$), or unfavourable ($R_L > 1$) [29].

The Freundlich isotherm is expressed in terms of the following Equation (5);

$$LogQ_e = \frac{1}{n} logC_e + logK_f \quad (5)$$

where Q_e is the adsorption capacity of the adsorbent (mg/g), C_e stands for the equilibrium concentration of adsorbate (mg/L). The K_f and n represent the adsorption strength and intensity respectively, and their values were calculated from the intercept and slope of Freundlich plot [28,29].

2.6. Desorption of arsenic

The regeneration capacity of the CuO/TiO_2 nanocomposite was investigated by performing a desorption experiment. For this purpose, 0.2 g of arsenic loaded nanocomposite was added to 0.5 M NaOH solution that is used as a desorbing agent and stirred in the solution for half an hour. The concentration of arsenic in the solution was determined after desorption. The desorption efficiency of the nanocomposite was calculated using the following Equation (6);

$$D = \frac{C_d - C_e}{C_0 - C_e} \times 100 \quad (6)$$

where D is the desorption efficiency and C_d is the concentration of adsorbate after desorption. C_0 and C_e represented the initial and equilibrium concentration of adsorbate, respectively. The regenerated nanocomposite was used again for the adsorption of As(V) and these desorption-adsorption experiments were repeated several times.

3. Results and discussion

3.1. Material characterization

3.1.1. XRD analysis

The XRD pattern of pure TiO_2, CuO and CuO/TiO_2 (1, 3 and 5 wt. %) nanocomposites is shown in Figure 1. The XRD spectra of TiO_2 represented in Figure 1a was compared with our previously reported work [30] which confirmed all of the peaks having 2θ value of 25.32, 37.8, 48.2, 53.9, 55.3, 62.9, and 69.01° matches the reflection in the (101), (004), (200), (105), (211), (204) and (116), respectively, crystal planes were presenting tetragonal geometry and anatase phase of TiO_2. The XRD spectra of CuO presented in Figure 1e was compared with the literature [31] which clearly showed that all the peaks having 2θ value of 32.31, 35.33, 38.74, 48.84, 53.43, 58.28, 61.43, 66.02, and 67.99° were corresponding to (110), (-111), (111), (-202), (020), (202), (-113), (022), and (113), respectively, crystal planes of the monoclinic phase of Tenorite CuO.

Table 1. Crystallite size and lattice parameter of the synthesized materials.

Material	Crystallite size (nm)	*d*-spacing (Å)	*a* (Å)	*b* (Å)	*c* (Å)
TiO_2	41.98	3.5122	3.7880	3.7880	9.5076
CuO	43.01	2.7368	4.6201	3.4232	5.0571
1wt. % CuO/TiO_2	42.09	3.5131	3.7878	3.7878	9.5172
3wt. % CuO/TiO_2	42.11	3.5136	3.8006	3.8006	9.5096
5wt. % CuO/TiO_2	41.75	3.5141	3.8046	3.8046	9.5252

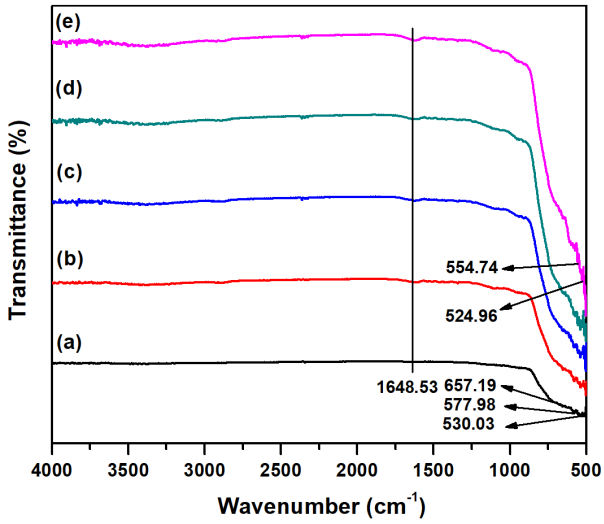

Figure 2. FTIR spectra of (a) TiO_2, (b) 1wt. % CuO/TiO_2, (c) 3wt. % CuO/TiO_2, (d) 5wt. % CuO/TiO_2 and (e) CuO.

The diffractograms of 1, 3 and 5 wt. % CuO/TiO_2 nanocomposites are presented in Figures 1b-d, clearly showing that all nanocomposite samples contain peaks similar to the anatase TiO_2. In addition, the diffraction peaks belonging to (-111) and (111) of the CuO crystal planes also appeared in spectra of 3 and 5 wt. % CuO/TiO_2 nanocomposites and become more prominent with 5 wt. % composition. There was no other peak appeared belonging to $Na_2Ti_3O_7$ or any other impurity which indicates that all of the nanocomposites primarily consist of tenorite CuO and anatase TiO_2 and the addition of CuO to TiO_2 did not cause any structural damages [32]. The average crystallite size calculated by the Debye-Scherrer equation and lattice parameters are given in Table 1. There was no significant change appearing in average crystallite size which also suggests that copper is present in the form of CuO rather than a metallic dopant.

3.1.2. FT-IR analysis

FT-IR spectra of calcined samples were presented in Figure 2. The FT-IR spectra of all CuO/TiO_2 nanocomposites showed a pattern similar to that of TiO_2. Each spectrum contains a broad region below 1000 cm^{-1} which represents the symmetric and asymmetric stretching and bending vibrational modes of M-O. The FTIR spectra of all nanocomposites contain characteristic peaks at 530 and 657 cm^{-1} which occur due to the stretching and bending modes of Ti-O-Ti that confirmed the formation of TiO_2 [33]. While peaks observed at 525 and 555 cm^{-1} were due to Cu-O stretching mode [31,34]. The peak that appeared at 1649 cm^{-1} represents the H-O-H flexion which may be due to either water or ethanol occluded in pores structure or due to hydroxyl group attached at the surface of TiO_2 structure (Ti-O-H) [35]. There was no other peak that appeared related to any impurity which signifies the purity of all calcined samples.

3.1.3. SEM analysis

The surface morphology and structural features of TiO_2, CuO, and 5 wt. % CuO/TiO_2 nanocomposite have been investigated by SEM as shown in Figure 3a-c, respectively. The SEM micrograph of TiO_2 shows that the nanoparticles are monodisperse and have a spherical geometry [36]. The SEM analysis of CuO presented in Figure 3b shows some agglomeration of particles due to a large surface area [37]. The homogeneous distribution of CuO over TiO_2 was observed in the SEM image of the nanocomposite, as illustrated in Figure 3c. The appearance of black colour on the surface of the nanocomposite was due to the presence of copper oxide nanoparticles. The average particle size of the nanocomposite was slightly higher than that of the TiO_2 nanoparticles due to some agglomeration of CuO with TiO_2, which confirmed the formation of the nanocomposite [36,38]. Due to the small size of CuO, there was no change appeared in the spherical geometry of nanocomposite.

3.2. Optimization of operating parameters for As(V) adsorption

On the basis of characterization results, we have selected 5 wt. % CuO/TiO_2 composite for optimization of different reaction parameters such as pH, contact time, adsorbent dose, and initial As(V) concentration due to its better composition, phase purity and textural features.

3.2.1. Effect of pH

The pH of the solution always plays a vital role in influencing the adsorption capacity of an adsorbent. The effect of pH on adsorption efficiency is much more pronounced than any other parameter because it directly concerns the surface charge of an adsorbent. It always increases adsorption by developing electrostatic attraction between oppositely charged surfaces of the adsorbent and pollutants. In addition to this, the type of arsenic species in the water will also vary with changes in pH [39]. The effect of pH on As(V) adsorption rate had been studied by varying in range of 1 to 9 (Operating conditions: C_0 = 100 ppb; 5 wt. % CuO/TiO_2 dose = 0.2 g; contact time = 2 hours; temperature = 298 K).

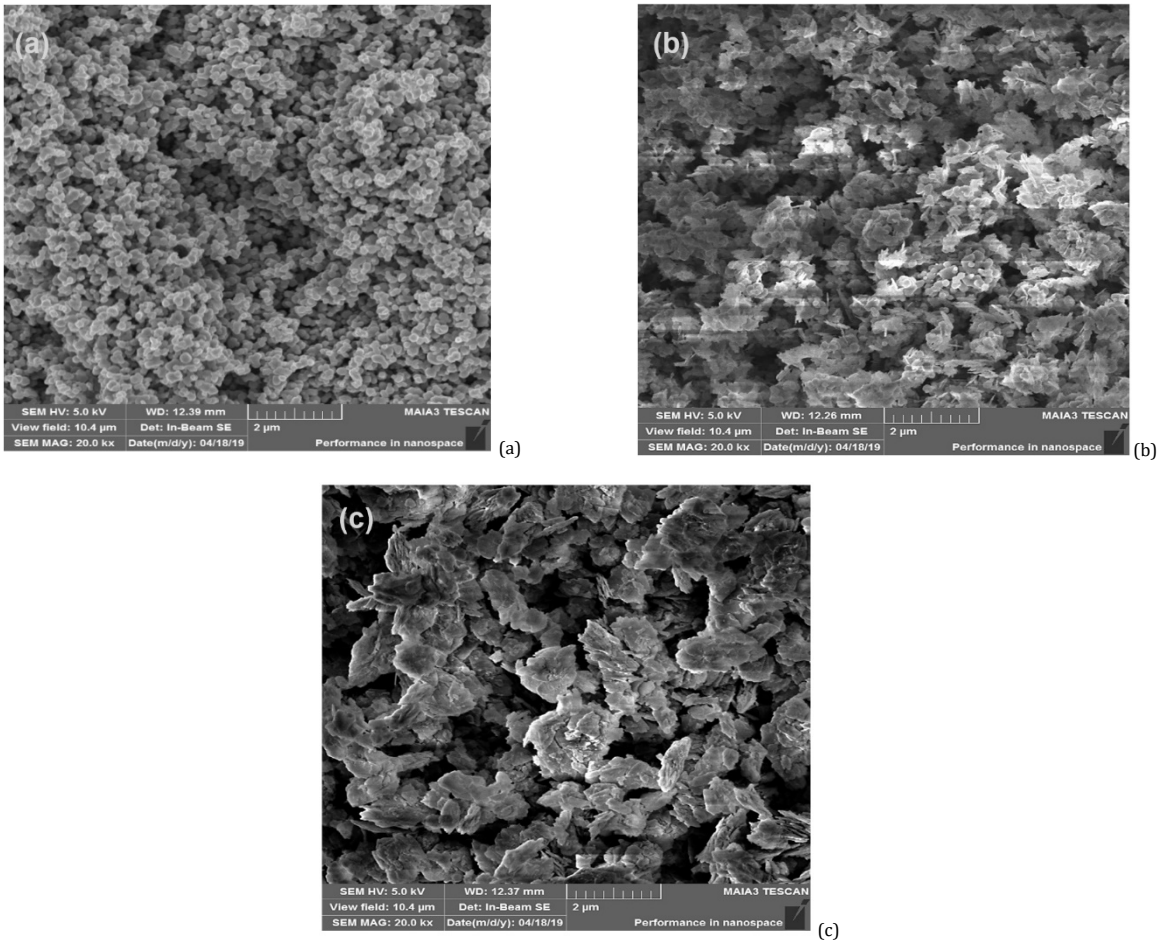

Figure 3. SEM images of (a) TiO_2, (b) CuO, (c) and 5wt. % CuO/TiO_2.

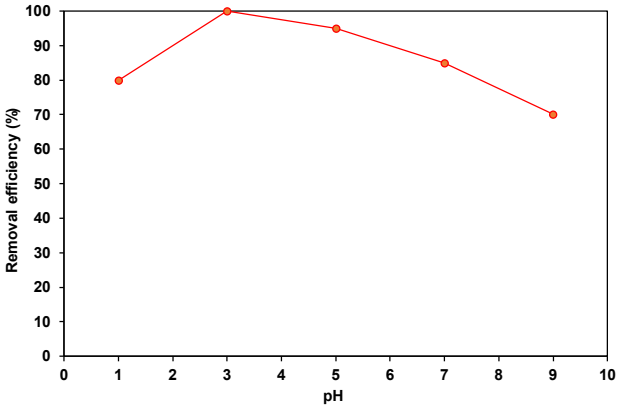

Figure 4. Effect of solution pH on As(V) adsorption rate on 5 wt. % CuO/TiO_2.

Figure 4 represents the variations in the % removal efficiency as a function of the pH of the solution. The result shows that the removal efficiency increased when the pH increased from 1 to 3. This is because, at pH = 3, $H_2AsO_4^{-1}$ is the only predominant As(V) species that exist in water and the surface of the nanocomposite is also protonated in an acid medium leading to a positively charged surface. This results in a strong electrostatic attraction between negatively charged arsenic species ($H_2AsO_4^{-1}$) and positively charged nanocomposite surfaces [40]. Further increase in pH leads to a decrease in removal efficiency. The possible reason for this is the increased electrostatic repulsion between negatively charged As(V) species ($H_2AsO_4^{-1}$ or $HAsO_4^{-2}$) and the negatively charged nanocomposite surface developed in basic medium. Therefore, the removal efficiency of the nanocomposite decreased at higher pH values [41]. The optimum value pH for As(V) removal was found to be 3.

3.2.2. Effect of contact time

The effectiveness of the adsorbent is also measured in terms of contact time. The dependence of % removal efficiency on contact time was investigated by varying time from 1 to 5 hours (Operating conditions: C_0 = 100 ppb; 5 wt. % CuO/TiO_2

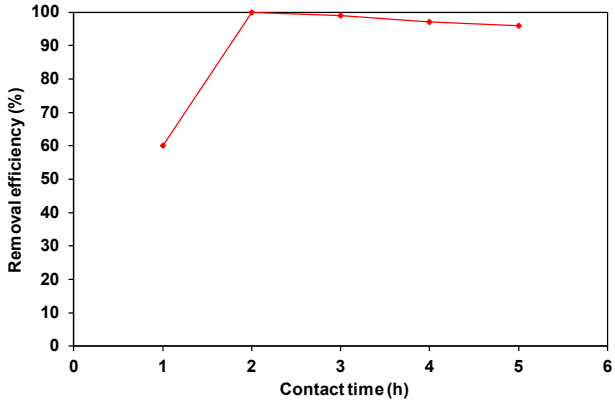

Figure 5. Effect of contact time on As(V) adsorption rate on 5 wt. % CuO/TiO_2.

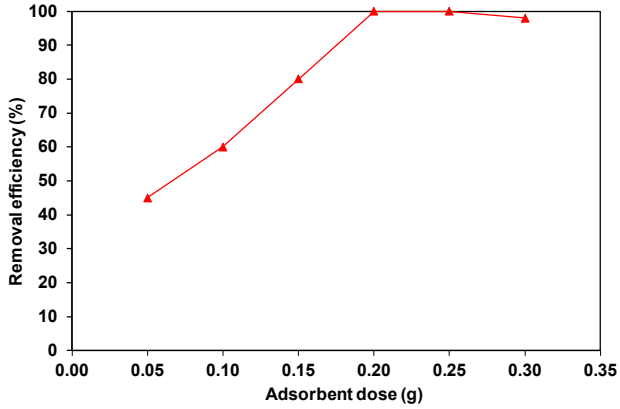

Figure 6. Effect of adsorbent dose on As(V) adsorption rate on 5 wt. % CuO/TiO_2.

dose = 0.2 g; pH = 3; temperature = 298 K) as shown in Figure 5. It was observed that the adsorption rate of As(V) increased sharply by the varying shaking time from 1 to 2 hours and become almost constant when the shaking time was further increased from 2 to 5 hours. It was concluded that equilibrium was established between the adsorbent and the adsorbate within the initial 2 hours. An increased shaking time did not show any effect on the equilibrium of arsenate adsorption on the nanocomposite surface [42]. This is because the surface area of the nanocomposite becomes rapidly saturated and no more sites are available for the adsorption of As(V) [43]. This result demonstrated the efficient affinity of the CuO/TiO_2 nanocomposite for As(V).

3.2.3. Effect of the nanocomposite dose

Studying the impact of adsorbent dose on adsorption capacity is way more pronounced in economic terms. The effect of nanocomposite dosage on As(V) removal rate had been studied by varying amounts of 5 wt. % CuO/TiO_2 nanocomposite from 0.05 to 0.3 g (Operating conditions: C_0 = 100 ppb; pH = 3; contact time = 2 hours; temperature = 298 K) as shown in Figure 6. The adsorption rate increased rapidly with an increase in the adsorbent dose to 0.2 g. It has been reported [36] that increased nanocomposite dose provides more active sites for As(V) adsorption which result in an enhanced adsorption rate. However, an additional increase in the dose of nanocomposites causes agglomeration of particles, as a result, decreasing the adsorption efficiency. Since the adsorption performance had not been improved with further increase in nanocomposite dose, therefore 0.2 g was considered as an optimized nanocomposite dose.

3.2.4. Effect of As(V) initial concentration

It is necessary from an industrial point of view to study the effect of the initial concentration of As(V) initial concentration on the adsorption rate. The effect of the initial concentration on its adsorption rate had been studied by varying the concentration of solution from 10 to 1000 ppb (Operating conditions: 5 wt. % CuO/TiO_2 dose = 0.2 g; pH = 3; contact time = 2 hours; temperature = 298 K) as shown in Figure 7. The result demonstrates that the adsorption of As(V) was not much affected by the increase in initial concentration. One of the possible reasons is that the presence of CuO in the nanocomposite enhanced the surface area, which results in higher adsorption capacity [44]. Moreover, the nanocomposite was found to be a promising candidate for the removal of As(V) at both very high and low concentration levels and can be employed for the treatment of contaminated drinking water where As(V) present at very low concentrations (10 ppb).

3.3. Isothermal studies

The adsorption isotherm developed an equilibrium relationship between the concentration of adsorbate in solution and at the surface of adsorbent at a constant temperature [45]. For this purpose, the initial As(V) concentration was varied from 10-1000 ppb (Operating conditions: 5 wt. % CuO/TiO_2 dose = 0.2 g; pH = 3; contact time = 2 hours; temperature = 298 K) to study the mechanism of As(V) adsorption on the surface of the nanocomposite. The well-known Langmuir and Freundlich adsorption isotherms were used to investigate the adsorption capacity of 5 wt. % CuO/TiO_2 nanocomposite.

Table 2. Calculated Langmuir parameters for 5 wt. % CuO/TiO_2 nanocomposite.

Langmuir parameters	% Removal efficiency
Q_{max}	90
r^2	0.9
R_L	0.9

Table 3. Calculated Freundlich parameters for 5 wt. % CuO/TiO_2 nanocomposite.

Freundlich parameters	% Removal efficiency
K_f	0.82
N	1
r^2	1

Table 4. Maximum adsorption capacity of various adsorbents for As(V) removal.

Adsorbent	Adsorption capacity (mg/g)	References
Nano-CuO & Nano-TiO_2	36.39 & 29.24	[47]
CuO	1.17	[48]
Fe_2O_3-MnO_2	16.6	[49]
γ- Fe_2O_3-TiO_2	33.03	[50]
Fe_2O_3@CuO&GO	62.60	[51]
Magnetic graphene oxide	69.44	[52]
5 wt. % CuO/TiO_2	90	This study

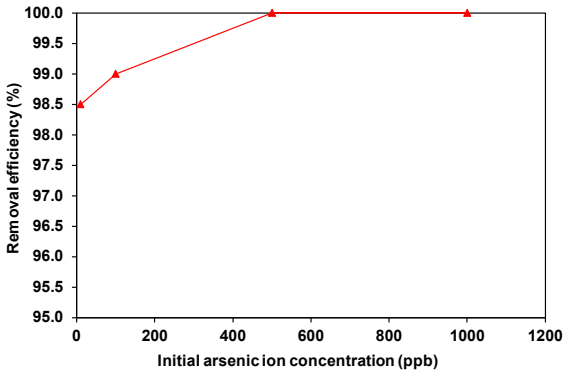

Figure 7. Effect of initial arsenic ion concentration on As(V) adsorption rate on 5 wt. % CuO/TiO_2.

3.3.1. Langmuir adsorption isotherm

The Langmuir isotherm presumed that monolayer adsorption takes place on the adsorbent surface having a finite number of indistinguishable sites [46]. The adsorption energy is not affected by the amount of surface coverage in this model. K and Q_{max} were determined using the slope ($1/Q_{max}$) and intercept ($1/KQ_{max}$) values obtained from the plot of C_e/Q_e against C_e. To ensure that As(V) is homogeneously adsorbed at the available nanocomposite sites, the R_L value was calculated from Equation (4). The R_L value and other calculated parameters are given in Table 2. The R_L value indicates that the As(V) adsorption over 5 wt % CuO/TiO_2 nanocomposite was favourable.

3.3.2. Freundlich adsorption isotherm

The Freundlich adsorption isotherms assumed that multilayer adsorption occurs on the surface of the adsorbent. This isotherm suggested that the ratio of adsorbate concentration at adsorbent surface to solution does not remain constant at different concentrations of solution [46]. The linear equation of Freundlich isotherm was used to determine K_f and other n for nanocomposite by plotting log (Q_e) against log(C_e). The calculated Freundlich parameters for 5 wt% CuO/TiO_2 nanocomposites are displayed in Table 3. Based on the correlation coefficient value (R^2), it has been clear that the Freundlich isotherm fits well to demonstrate the adsorption mechanism of As(V) on the nanocomposite surface. For favorable adsorption, the value of Freundlich's constant "n" must be in the range of 1-10 [45]. As the value of "n" was found high enough to indicate the better separation of As(V) from the aqueous solution, so it was suggested that the physical adsorption occurs, and the nanocomposite possesses a high affinity for As(V). The value of Freundlich parameters demonstrated adsorption capacity of the 5 wt. % CuO/TiO_2 nanocomposite has been found greater for As(V).

3.4 Regeneration of nanocomposite

The low removal efficiency of As(V) at pH = 9 implied that adsorbed arsenic ion can be effectively removed from the surface of 5 wt. % CuO/TiO_2 nanocomposite in basic medium. In a basic medium, the surface of the nanocomposite becomes negatively charged due to the increase in hydroxyl ions, which results in the desorption of negatively charged arsenate species ($H_2AsO_4^{-1}$ or $HAsO_4^{-2}$) [41]. The presence of NaOH in solution causes rapid de-protonation of nanocomposite surface which causes a rapid increase in the desorption rate of As(V). For this purpose, As(V) loaded CuO/TiO_2 nanocomposite was stirred for one hour in 0.5 M NaOH solution. The adsorption and desorption efficiency of the nanocomposite was calculated from Equations (1) and (6) and the values are presented in Figure 8. The As(V) adsorption and desorption rate on the surface of 5 wt. % CuO/TiO_2 nanocomposite remained almost constant during each run of the desorption-adsorption cycles.

3.5. Comparison of adsorption capacity of 5 wt. % CuO/TiO_2 nanocomposite with already reported adsorbents

The maximum adsorption capacity of 5 wt. % CuO/TiO_2 nanocomposite and other adsorbents for As(V) removal are summarized in Table 4 which compares the adsorption capacity of 5 wt. % CuO/TiO_2 nanocomposite with that of other

adsorbents reported in the literature, as calculated from Langmuir isotherm. The results in Table 4 demonstrate that 5 wt. % CuO/TiO_2 nanocomposite provided higher adsorption capacity for As(V) removal than several other adsorbents reported in the literature.

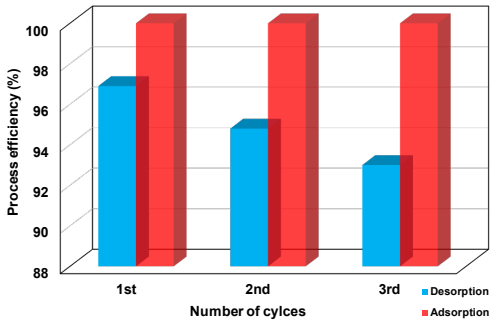

Figure 8. Desorption and adsorption efficiencies of 5 wt. % CuO/TiO_2 nanocomposite.

4. Conclusion

Cost-effective CuO/TiO_2 nanocomposites (1, 3 and 5 wt. %) having enhanced surface area and high adsorption capacity were prepared by the precipitation-deposition method. Important parameters such as pH, contact time, arsenic ion concentration, and nanocomposite dose were optimized to enhance As(V) adsorption over the CuO/TiO_2 nanocomposite. The results of Langmuir and Freundlich isotherms investigations indicate that Freundlich adsorption isotherm produces the best fit. The nanocomposite was successfully regenerated by treatment with NaOH solution and can be reused for three cycles without any prominent loss in adsorption efficiency. The CuO/TiO_2 nanocomposite showed remarkable adsorption efficiency in arsenic decontamination.

Acknowledgment

The authors are highly thankful to Quaid-i-Azam University, Islamabad and National Centre for Physics, Islamabad Pakistan for providing the chemicals, laboratory facilities and sample characterization for this project.

Disclosure statement

Conflict of interests: The authors declare that they have no conflict of interest.
Ethical approval: All ethical guidelines have been adhered.
Sample availability: Samples of the compounds are available from the author.

CRediT authorship contribution statement

Conceptualization: Saima Farooq, Sobia Ashraf; Methodology: Asima Siddiqa, Sobia Ashraf; Validation: Shabnam Shahida, Sara Qaisar; Formal Analysis: Saiqa Imran, Sara Qaisar; Investigation: Sobia Ashraf, Sabtain Haider; Data Curation: Sabtain Haider; Writing - Original Draft: Saima Farooq, Sabtain Haider; Writing - Review and Editing: Saiqa Imran, Asima Siddiqa; Supervision: Shabnam Shahida; Project Administration: Asima Siddiqa.

ORCID and Email

Saima Farooq
saima@unizwa.edu.om
https://orcid.org/0000-0002-5037-0769
Asima Siddiqa
a.sam.malik@gmail.com
https://orcid.org/0000-0002-3087-8047
Sobia Ashraf
sobiakhanashraf@gmail.com
https://orcid.org/0000-0002-8744-6317
Sabtain Haider
hsibtain04@gmail.com
https://orcid.org/0000-0002-7405-4824
Saiqa Imran
saiqa134@gmail.com
https://orcid.org/0000-0002-0289-4736
Shabnam Shahida
shabnamshahida@upr.edu.pk
https://orcid.org/0000-0001-9861-4569
Sara Qaisar
sara.qaisar@ncp.edu.pk
https://orcid.org/0000-0002-3724-9665

References

[1]. Shaji, E.; Santosh, M.; Sarath, K. V.; Prakash, P.; Deepchand, V.; Divya, B. V. Arsenic contamination of groundwater: A global synopsis with focus on the Indian Peninsula. *Geosci. front.* **2021**, *12*, 101079.
[2]. Wongsasuluk, P.; Chotpantarat, S.; Siriwong, W.; Robson, M. Human biomarkers associated with low concentrations of arsenic (As) and lead (Pb) in groundwater in agricultural areas of Thailand. *Sci. Rep.* **2021**, *11*, 13896.
[3]. Moreira, V. R.; Lebron, Y. A. R.; Santos, L. V. S.; Coutinho de Paula, E.; Amaral, M. C. S. Arsenic contamination, effects and remediation techniques: A special look onto membrane separation processes. *Process Saf. Environ. Prot.* **2021**, *148*, 604–623.
[4]. Fischer, A.; Lee, M.-K.; Ojeda, A. S.; Rogers, S. R. GIS interpolation is key in assessing spatial and temporal bioremediation of groundwater arsenic contamination. *J. Environ. Manage.* **2021**, *280*, 111683.
[5]. Murcott, S. Arsenic Contamination in the World: An International Sourcebook 2012. *Water Intell. Online* **2012**, *11*.
[6]. Siddiq, O. M.; Tawabini, B. S.; Soupios, P.; Ntarlagiannis, D. Removal of arsenic from contaminated groundwater using biochar: a technical review. *Int. J. Environ. Sci. Technol. (Tehran)* **2022**, *19*, 651–664.
[7]. Nicomel, N. R.; Leus, K.; Folens, K.; Van Der Voort, P.; Du Laing, G. Technologies for arsenic removal from water: Current status and future perspectives. *Int. J. Environ. Res. Public Health* **2015**, *13*, 62.
[8]. Shishu, K. K.; Das Ambika, B. Depression, anxiety and stress among arsenic-induced cancer patients in Indo-Gangetic plains of Bihar: Role of proactive coping. *Int. Q. Community Health Educ.* **2021**, 0272684X2110334.
[9]. Huang, H.-W.; Lee, C.-H.; Yu, H.-S. Arsenic-induced carcinogenesis and immune dysregulation. *Int. J. Environ. Res. Public Health* **2019**, *16*, 2746.
[10]. Shankar, S.; Shanker, U.; Shikha Arsenic contamination of ground water: a review of sources, prevalence, health risks, and strategies for mitigation. *ScientificWorldJournal* **2014**, *2014*, 304524.
[11]. Kong, L.; Wang, Y.; Andrews, C. B.; Zheng, C. One-step construction of hierarchical porous channels on electrospun MOF/polymer/graphene oxide composite nanofibers for effective arsenate removal from water. *Chem. Eng. J.* **2022**, *435*, 134830.
[12]. Sorlini, S.; Gialdini, F. Conventional oxidation treatments for the removal of arsenic with chlorine dioxide, hypochlorite, potassium permanganate and monochloramine. *Water Res.* **2010**, *44*, 5653–5659.
[13]. Linh, H. X.; Oanh, P. T.; Huy, N. N.; Van Hao, P.; Ngoc Minh, P.; Hong, P. N.; Van Thanh, D. Electrochemical mass production of graphene nanosheets for arsenic removal from aqueous solutions. *Mater. Lett.* **2019**, *250*, 16–19.
[14]. Litter, M. I.; Morgada, M. E.; Bundschuh, J. Possible treatments for arsenic removal in Latin American waters for human consumption. *Environ. Pollut.* **2010**, *158*, 1105–1118.
[15]. Sun, Y.; Yu, I. K. M.; Tsang, D. C. W.; Cao, X.; Lin, D.; Wang, L.; Graham, N. J. D.; Alessi, D. S.; Komárek, M.; Ok, Y. S.; Feng, Y.; Li, X.-D. Multifunctional iron-biochar composites for the removal of potentially toxic elements, inherent cations, and hetero-chloride from hydraulic fracturing wastewater. *Environ. Int.* **2019**, *124*, 521–532.
[16]. Asere, T. G.; Stevens, C. V.; Du Laing, G. Use of (modified) natural adsorbents for arsenic remediation: A review. *Sci. Total Environ.* **2019**, *676*, 706–720.
[17]. Yeo, K. F. H.; Li, C.; Zhang, H.; Chen, J.; Wang, W.; Dong, Y. Arsenic removal from contaminated water using natural adsorbents: A review. *Coatings* **2021**, *11*, 1407.
[18]. Lingamdinne, L. P.; Lee, S.; Choi, J.-S.; Lebaka, V. R.; Durbaka, V. R. P.; Koduru, J. R. Potential of the magnetic hollow sphere nanocomposite (graphene oxide-gadolinium oxide) for arsenic removal from real field water and antimicrobial applications. *J. Hazard. Mater.* **2021**, *402*, 123882.
[19]. Guan, X.; Du, J.; Meng, X.; Sun, Y.; Sun, B.; Hu, Q. Application of titanium dioxide in arsenic removal from water: A review. *J. Hazard. Mater.* **2012**, *215–216*, 1–16.

[20]. Feng, C.; Aldrich, C.; Eksteen, J. J.; Arrigan, D. W. M. Removal of arsenic from alkaline process waters of gold cyanidation by use of Fe3O4@SiO2@TiO2 nanosorbents. *Miner. Eng.* **2017**, *110*, 40–46.

[21]. Sagharloo, N. G.; Rabani, M.; Salimi, L.; Ghafourian, H.; Sadatipour, S. M. T. Immobilized ZnO/TiO2 activated carbon (I ZnO/TiO2 AC) to removal of arsenic from aqueous environments: optimization using response surface methodology and kinetic studies. *Biomass Convers. Biorefin.* **2021**, 10.1007/s13399-021-01741–1.

[22]. Malwal, D.; Gopinath, P. Rapid and efficient removal of arsenic from water using electrospun CuO–ZnO composite nanofibers. *RSC Adv.* **2016**, *6*, 115021–115028.

[23]. Sharma, M.; Poddar, M.; Gupta, Y.; Nigam, S.; Avasthi, D. K.; Adelung, R.; Abolhassani, R.; Fiutowski, J.; Joshi, M.; Mishra, Y. K. Solar light assisted degradation of dyes and adsorption of heavy metal ions from water by CuO–ZnO tetrapodal hybrid nanocomposite. *Mater. Today Chem.* **2020**, *17*, 100336.

[24]. Bhattacharya, P.; Mukherjee, D.; Dey, S.; Ghosh, S.; Banerjee, S. Development and performance evaluation of a novel CuO/TiO2 ceramic ultrafiltration membrane for ciprofloxacin removal. *Mater. Chem. Phys.* **2019**, *229*, 106–116.

[25]. Xiaoyuan, J.; Guanghui, D.; Liping, L.; Yingxu, C.; Xiaoming, Z. Catalytic activities of CuO/TiO2 and CuO-ZrO2/TiO2 in NO + CO reaction. *J. Mol. Catal. A Chem.* **2004**, *218*, 187–195.

[26]. Mahimairaja, S.; Bolan, N. S.; Adriano, D. C.; Robinson, B. Arsenic contamination and its risk management in complex environmental settings. In *Advances in Agronomy*; Elsevier, 2005; pp. 1–82.

[27]. Thotagamuge, R.; Kooh, M. R. R.; Mahadi, A. H.; Lim, C. M.; Abu, M.; Jan, A.; Hanipah, A. H. A.; Khiong, Y. Y.; Shofry, A. Copper modified activated bamboo charcoal to enhance adsorption of heavy metals from industrial wastewater. *Environ. Nanotechnol. Monit. Manag.* **2021**, *16*, 100562.

[28]. Neag, E.; Malschi, D.; Măicăneanu, A. Isotherm and kinetic modelling of Toluidine Blue (TB) removal from aqueous solution using Lemna minor. *Int. J. Phytoremediation* **2018**, *20*, 1049–1054.

[29]. Farooq, S.; Al Maani, A. H.; Naureen, Z.; Hussain, J.; Siddiqa, A.; Al Harrasi, A. Synthesis and characterization of copper oxide-loaded activated carbon nanocomposite: Adsorption of methylene blue, kinetic, isotherm, and thermodynamic study. *J. Water Proc.engineering* **2022**, *47*, 102692.

[30]. Siddiqa, A.; Masih, D.; Anjum, D.; Siddiq, M. Cobalt and sulfur co-doped nano-size TiO2 for photodegradation of various dyes and phenol. *J. Environ. Sci. (China)* **2015**, *37*, 100–109.

[31]. Ilkhechi, N. N.; Koozegar-Kaleji, B.; Dousi, F. Optical and structural properties of tenorite nanopowders doped by Si and Zr. *Opt. Quantum Electron.* **2015**, *47*, 633–642.

[32]. Kolaei, M.; Tayebi, M.; Lee, B.-K. The synergistic effects of acid treatment and silver (Ag) loading for substantial improvement of photoelectrochemical and photocatalytic activity of Na2Ti3O7/TiO2 nanocomposite. *Appl. Surf. Sci.* **2021**, *540*, 148359.

[33]. Bibi, S.; Ahmad, A.; Anjum, M. A. R.; Haleem, A.; Siddiq, M.; Shah, S. S.; Kahtani, A. A. Photocatalytic degradation of malachite green and methylene blue over reduced graphene oxide (rGO) based metal oxides (rGO-Fe3O4/TiO2) nanocomposite under UV-visible light irradiation. *J. Environ. Chem. Eng.* **2021**, *9*, 105580.

[34]. Bouazizi, N.; Bargougui, R.; Oueslati, A.; Benslama, R. Effect of synthesis time on structural, optical and electrical properties of CuO nanoparticles synthesized by reflux condensation method. *Adv. Mater. Lett.* **2015**, *6*, 158–164.

[35]. Shi, X. Z.; Gu, Y.; Liu, T. Y.; Jiang, Z. H.; Li, R.; Zeng, F. Effect of different P2O5/SnF2 ratios on the structure and properties of phosphate glass. *J. Non Cryst. Solids* **2022**, *578*, 121350.

[36]. Nekooie, R.; Shamspur, T.; Mostafavi, A. Novel CuO/TiO2/PANI nanocomposite: Preparation and photocatalytic investigation for chlorpyrifos degradation in water under visible light irradiation. *J. Photochem. Photobiol. A Chem.* **2021**, *407*, 113038.

[37]. Dulta, K.; Koşarsoy Ağçeli, G.; Chauhan, P.; Jasrotia, R.; Chauhan, P. K.; Ighalo, J. O. Multifunctional CuO nanoparticles with enhanced photocatalytic dye degradation and antibacterial activity. *Sustain. Environ. Res.* **2022**, *32*.

[38]. Lu, D.; Zelekew, O. A.; Abay, A. K.; Huang, Q.; Chen, X.; Zheng, Y. Synthesis and photocatalytic activities of a CuO/TiO2 composite catalyst using aquatic plants with accumulated copper as a template. *RSC Adv.* **2019**, *9*, 2018–2025.

[39]. Wei, Z.; Liang, K.; Wu, Y.; Zou, Y.; Zuo, J.; Arriagada, D. C.; Pan, Z.; Hu, G. The effect of pH on the adsorption of arsenic(III) and arsenic(V) at the TiO 2 anatase [1 0 1] surface. *J. Colloid Interface Sci.* **2016**, *462*, 252–259.

[40]. Tao, L.; Huang, M.; Li, H.; Chen, W.; Su, Z.; Guan, Y. Cadmium and arsenic interactions under different molar ratios during coadsorption processes by excluding pH interference. *Chemosphere* **2022**, *291*, 132839.

[41]. Yeo, K. F. H.; Li, C.; Dong, Y.; Yang, Y.; Wu, K.; Zhang, H.; Chen, Z.; Gao, Y.; Wang, W. Adsorption performance of Fe(III) modified kapok fiber for As(V) removal from water. *Sep. Purif. Technol.* **2022**, *287*, 120494.

[42]. Sajjadi, S.-A.; Meknati, A.; Lima, E. C.; Dotto, G. L.; Mendoza-Castillo, D. I.; Anastopoulos, I.; Alakhras, F.; Unuabonah, E. I.; Singh, P.; Hosseini-Bandegharaei, A. A novel route for preparation of chemically activated carbon from pistachio wood for highly efficient Pb(II) sorption. *J. Environ. Manage.* **2019**, *236*, 34–44.

[43]. Naushad, M.; Alqadami, A. A.; AlOthman, Z. A.; Alsohaimi, I. H.; Algamdi, M. S.; Aldawsari, A. M. Adsorption kinetics, isotherm and reusability studies for the removal of cationic dye from aqueous medium using arginine modified activated carbon. *J. Mol. Liq.* **2019**, *293*, 111442.

[44]. Sharma, A.; Lee, B.-K. Growth of TiO 2 nano-wall on activated carbon fibers for enhancing the photocatalytic oxidation of benzene in aqueous phase. *Catal. Today* **2017**, *287*, 113–121.

[45]. Urbano, B. F.; Villenas, I.; Rivas, B. L.; Campos, C. H. Cationic polymer–TiO2 nanocomposite sorbent for arsenate removal. *Chem. Eng. J.* **2015**, *268*, 362–370.

[46]. Seema, K. M.; Mamba, B. B.; Njuguna, J.; Bakhtizin, R. Z.; Mishra, A. K. Removal of lead (II) from aqeouos waste using (CD-PCL-TiO2) bio-nanocomposites. *Int. J. Biol. Macromol.* **2018**, *109*, 136–142.

[47]. Zhan, H.; Jiang, Y.; Ma, Q. Determination of adsorption characteristics of metal oxide nanomaterials: Application as adsorbents. *Anal. Lett.* **2014**, *47*, 871–884.

[48]. Saif, S.; Adil, S. F.; Khan, M.; Hatshan, M. R.; Khan, M.; Bashir, F. Adsorption studies of arsenic(V) by CuO nanoparticles synthesized by Phyllanthus emblica leaf-extract-fueled solution combustion synthesis. *Sustainability* **2021**, *13*, 2017.

[49]. Viswan, A.; Gangadharan, D. Adsorptive remediation of organic pollutant and arsenic (V) ions from water using Fe3O4-MnO2 nanocomposite. *Nano-struct. nano-objects* **2022**, *29*, 100837.

[50]. Yu, L.; Peng, X.; Ni, F.; Li, J.; Wang, D.; Luan, Z. Arsenite removal from aqueous solutions by γ-Fe2O3-TiO2 magnetic nanoparticles through simultaneous photocatalytic oxidation and adsorption. *J. Hazard. Mater.* **2013**, *246–247*, 10–17.

[51]. Wu, K.; Jing, C.; Zhang, J.; Liu, T.; Yang, S.; Wang, W. Magnetic Fe3O4@CuO nanocomposite assembled on graphene oxide sheets for the enhanced removal of arsenic(III/V) from water. *Appl. Surf. Sci.* **2019**, *466*, 746–756.

[52]. Thy, L. T. M.; Thuong, N. H.; Tu, T. H.; My, N. H. T.; Tuong, H. H. P.; Nam, H. M.; Phong, M. T.; Hieu, N. H. Fabrication and adsorption properties of magnetic graphene oxide nanocomposites for removal of arsenic (V) from water. *Adsorp. Sci. Technol.* **2020**, *38*, 240–253.